Supplementary Materials

A Broadly Neutralizing Antibody Inhibits SARS-CoV-2 Variants Through a Novel Mechanism of Disrupting Spike Trimer Integrity

Yunping Ma[1,2#], Qiyu Mao[1#], Yingdan Wang[1#], Zhaoyong Zhang[3#], Jiali Chen[1], Aihua Hao[1], Palizhati Rehati[1], Yanqun Wang[3], Yumei Wen[1], Lu Lu[1], Zhenguo Chen[1], Jincun Zhao[3,4*], Fan Wu[2*], Lei Sun[1*], Jinghe Huang[1*]

[1]Key Laboratory of Medical Molecular Virology (MOE/NHC/CAMS) and Shanghai Institute of Infectious Disease and Biosecurity, Shanghai Public Health Clinical Center, Shanghai Fifth People's Hospital, Institutes of Biomedical Sciences, School of Basic Medical Sciences, Fudan University, Shanghai, China.
[2]Shanghai Immune Therapy Institute, Shanghai Jiao Tong University School of Medicine Affiliated Renji Hospital, Shanghai, China.
[3]State Key Laboratory of Respiratory Disease, National Clinical Research Center for Respiratory Disease, Guangzhou Institute of Respiratory Health, the First Affiliated Hospital of Guangzhou Medical University, Guangzhou, Guangdong, China;
[4]Shanghai Institute for Advanced Immunochemical Studies, School of Life Science and Technology, ShanghaiTech University, Shanghai, China

[#]These authors contributed equally: Yunping Ma, Qiyu Mao, Yingdan Wang, Zhaoyong Zhang

*Correspondence: Jincun Zhao (zhaojincun@gird.cn), Fan Wu (wufan@fudan.edu.cn), Lei Sun (llsun@fudan.edu.cn), Jinghe Huang (Jinghehuang@fudan.edu.cn)

Keywords: COVID-19; SARS-CoV-2; Neutralizing Ab; Omicron BQ.1.1 and XBB.1.16

Materials and Methods

Cell lines, participants

Huh-7 cells and 293T cells were maintained in Dulbecco's Modified Eagle Medium (DMEM) supplemented with 10% fetal bovine serum (FBS), 1,000 units/mL penicillin and 1,000 μg/mL streptomycin. All cell lines were cultured at 37℃ in 5% CO2. HEK293F suspension cells were maintained in serum free SMM 293-TII Expression Medium (Sino Biological Inc.), and cultured at 37℃ in 5% CO2 with shaking at 120rpm. The study protocol was approved by the Ethics Committee of the Shanghai Public Health Clinical Center (YJ-2020-S021-01). Written informed consent approved by the Institutional Review Board was signed by all participants.

RBD Proteins Generation

Sequence of RBD protein (residues Arg319-phe541) were synthesized (GenScript), and cloned into pSecTag expression vectors with 8×His tag at C-terminal. HEK293F suspension cells were transiently tranfected with recombinant RBD expression plasmid using Ez Trans reagent (Life-iLab, China). Five days after transfection, the media was collected by centrifugation, followed by purification using Ni Sepharose High performance (GE health) following manufacturers' protocol.

Production of Pseudoviruses

The spike genes of the wild-type SARS-CoV-2 strain and the Alpha (B.1.1.7), Beta (B.1.351), Delta (B.1.617.2), BA.1, BA.2.12.1, BA.2.75, and BA.5 variants were synthesized and cloned into the pcDNA3.1 vector. Plasmids containing the spike genes of the BA.2.75 and BA.5 subvariants were generated from the pcDNA3.1-BA.2.75-Spike and pcDNA3.1-BA.5-Spike plasmids, respectively, using site-directed mutagenesis. Oligonucleotides complementary to the template and containing the targeted substitutions were synthesized. Plasmids

with specific mutations in the spike gene were produced through PCR-based cloning. The pseudovirus plasmids and the pNL4-3.Luc.R-E- backbone plasmid were transiently co-transfected into HEK293T cells using Ez Trans transfection reagent (Life-iLab, China), and the culture medium was changed to fresh growth medium (DMEM supplemented with 10% FBS). After 48 hours, the supernatants were collected, stored at -80°C, and subsequently thawed for use in pseudovirus neutralization assays.

Memory B cells sorting and antibody cloning, sequencing and production

B cells labeling and sorting were performed as previously described[1]. In brief, peripheral blood from patients was collected, and peripheral blood mononuclear cells (PBMCs) were isolated by density gradient centrifugation with Ficoll-Paque. Memory B lymphocytes (CD19+IgA-IgD-IgM-) were negatively selected, suspended in interleukin-2 (IL-2), IL-21, and irradiated 3T3-msCD40L cells. The cells were then sorted into 386-well plates, and supernatants were collected after 14 days to assess neutralizing activity against SARS-CoV-2. Antibody cloning and sequencing were performed as previously reported[2-4]. The somatic hypermutation rate (SHM) and CDRH3 sequence were determined using IMGT/V-QUEST. The variable regions of the heavy chain (VH) and light chain (VL) of the monoclonal antibodies (mAbs) were inserted into IgG1 antibody expression vectors. The heavy chain and light chain expression plasmids were transiently co-transfected into HEK293F cells, supernatants were harvested after 5 days, and antibodies were purified using protein G beads.

Pseudovirus Neutralization assay

The neutralization assay was performed as previously described[5,6]. In brief, Huh-7 cells were seeded in 96-well plates with growth medium (DMEM supplemented with 10% FBS) 12 hours before pseudovirus infection. Monoclonal antibodies (10 μL of 5-fold serial dilutions in growth medium) were

incubated with pseudovirus (40 μL) for 30 minutes at 37°C and then added to the cells. Background control wells received 50 μL of growth medium, and virus control wells received 10 μL of growth medium and 40 μL of pseudovirus. After 24 hours of infection, the cells were replenished with 150 μL of fresh growth medium. Following an additional 24 hours of incubation, the supernatants were aspirated, and the Huh-7 cells were lysed to assess luciferase expression (PerkinElmer EnSight). The inhibition rate was calculated using the following equation:

$$\%\text{Neut} = \frac{(\text{average RLU of virus control} - \text{RLU of sample})}{(\text{average RLU of virus control} - \text{average RLU of background})} * 100$$

Neutralization IC50 were determined by a “Sigmoidal dose-response with absolute IC50 IC80” regression in GraphPad Prism 9.

ELISA

To assess the binding of monoclonal antibodies to the receptor-binding domain (RBD) of SARS-CoV-2 variants, recombinant RBD proteins were immobilized on 96-well ELISA plates at 1-3 μg/mL in 100 μL at 4°C overnight. After blocking with non-fat milk in PBS, serial 5-fold dilutions of the monoclonal antibodies were added to the plates and incubated for 60 minutes at 37°C. The plates were washed with PBST, and a secondary antibody (goat anti-human IgG-HRP) was added. ABTS was added, and antibody binding was determined by measuring absorbance at 405 nm using a microplate reader.

Biolayer interferometry (BLI) binding assay

Antibody binding affinities were determined using an Octet-RED96 system (FortéBio) with NTA biosensors. PBST (0.05% Tween-20 in PBS) was used as the running buffer. Antibodies and proteins were diluted in PBST beforehand. Recombinant RBDs of the variants were captured on the NTA sensor at 10 μg/mL. After a baseline measurement for 200 seconds, the sensors were immersed in 3-fold serial dilutions of the monoclonal antibodies for 300 seconds.

This was followed by immersion in buffer alone for 300 seconds. After each association and dissociation cycle, the sensors were regenerated using 10 mM glycine-HCl (pH 1.5). The buffer well served as a negative control, and nonspecific binding was normalized by subtracting the signal from the dataset. The binding affinity of the monoclonal antibodies was calculated using a 1:1 binding model with the FortéBio Data Analysis 8.1 software.

ACE2 competition binding assay by BLI

The recombinant human angiotensin-converting enzyme 2 (hACE2) protein used in this study comprised residues Met1 to Ser740 fused to the Fc portion of human IgG1 at the C-terminus. For the ACE2 competition assay, hACE2-Fc was loaded onto an anti-human Fc (AHC) biosensor for 300 seconds at 20 μg/mL. After a baseline measurement for 200 seconds, the biosensors were exposed to 50 μg/mL of an IgG1 isotype control antibody to block any unoccupied sites on the sensors for 600 seconds. The biosensors were then added to wells containing a pre-mixture of 100 nM RBD protein and 600 nM monoclonal antibodies for 300 seconds. The binding response was recorded at each step. An irrelevant antibody was used as a negative control, and hACE2-Fc alone was used as a positive control competitor.

Antibody-dependent enhancement of SARS-CoV-2 variants infection

To assess antibody-dependent enhancement (ADE) of SARS-CoV-2 variant infection, we utilized a pseudotyped virus assay as previously described.[7] Pseudotyped viruses expressing the spike proteins of SARS-CoV-2 variants were incubated with serial 5-fold dilutions of antibody for 1 hour at 37°C. The antibody-pseudovirus mixtures containing approximately 100,000 relative light units (RLU) were then added to Raji B cells adhered to poly-L-lysine-coated 96-well plates. Following 24 hours of incubation at 37°C, the supernatant was replaced with fresh medium. After an additional 48 hours, luciferase substrate was added to lyse the cells and quantify RLUs using a microplate reader per

the manufacturer's protocol (Promega).

Animal experiments

The prophylactic and therapeutic efficacy of the monoclonal antibody 6i18 was evaluated in vivo using 6- to 8-week-old BALB/c mice. As previously described[8], mice received either 200 μg of 6i18 (10 mg/kg) intraperitoneally (i.p.) or 20 μg of 6i18 (1 mg/kg) intranasally (i.n.), either 24 hours before or after challenge with 1×10^5 focus-forming units (FFU) of the SARS-CoV-2 XBB.1 variant. Mice treated with phosphate-buffered saline (PBS) and challenged with an equivalent dose of the XBB.1 variant served as negative controls. The pulmonary viral burden was assessed by collecting lung samples 48 hours post-infection and quantifying infectious virus using a focus formation assay (FFA).

Formation of XBB S-6i18 complex

The purified XBB S trimer was mixed with 6i18 at a 1:1.5 molar ratio, incubated at 4℃ for 1h, and further purified by gel filtration. The peak fraction of the gel filtration was further analyzed by negative stain and cryo-EM.

Cryo-EM data collection and image processing

Cryo-EM data of XBB.1 S with 6i18 antibody was collected using TITAN Krios G4 transmission electron microscope (Thermo Fisher) operating at 300kV equipped with Falcon 4i and Selectries X Imaging filter with a slit width of 20eV. EER Movie stacks in AFIS mode were automatically collected using EPU software in super resolution mode at a nominal magnification 130,000x, physical pixel size of 0.932Å, a defocus range of -1.0 μm to -3.0 μm, dose fractioned to 1080 frames with a total dose of ~50e^-/Å^2.

All micrographs were binned 2x2, dose weighted and motion corrected in Relion v3.1[9], then the contrast transfer function (CTF) was estimated with Gctf[10]. All motion corrected micrographs were imported to cryoSPARC v4.0.3 for further

patched CTF-estimation and Manually Curate Exposures[11]. Bad exposures were discarded based upon ice condition, astigmatism and estimated resolution, and a total of 2,915 micrographs were selected for further blob picking, template picking and 2D classification. Good particles were selected for ab-initio, yeilding a map of XBB.1 monomer's NTD, RBD, complexed with one Fab, while density other domains is absent. The resulting volume were used for Create Templates and a new round of template picking, then particles from three rounds of picking were merged and de-duplicated and a total particle stack of 662,816 particles were imported to Relion through pyem package[12]. One round of 3D classification of global search yielded 518,597 good particles, and exported back to cryoSPARC for Local Refine to a final resolution of 3.34 Å, the map was postprocessed with deepEMhancer[13]. 3DFSC Program Suite Version 3.0[14] was used to estimate the resolution. Maps are evaluated in UCSF Chimera[15]. The above data processing procedures are summarized in Supplementary information Figure 2.

Model building and refinement

XBB.1 S monomer model was fitted with cryoEM model of Omicron S (PDB ID: 7WOW), and 6i18 antibody model was generated with Protein Folding function using Hermite® Platform (https://hermite.dp.tech,DP Technology) and then fitted into the density with UCSF Chimera. Further manual adjustments were performed in COOT and after which, real space refinement was carried out in PHENIX[16,17]. Model validation was performed using MolProbity. Figures were prepared using UCSF Chimera and UCSF ChimeraX. The statistics of model refinement and data collection are listed in Supplementary information Table S2.

References

1 Huang, J. *et al.* Isolation of human monoclonal antibodies from peripheral blood B cells. *Nature protocols* **8**, 1907-1915, doi:10.1038/nprot.2013.117 (2013).

2 Huang, J. *et al.* Identification of a CD4-Binding-Site Antibody to HIV that Evolved Near-

Pan Neutralization Breadth. *Immunity* **45**, 1108-1121, doi:10.1016/j.immuni.2016.10.027 (2016).

3 Huang, J. *et al.* Broad and potent HIV-1 neutralization by a human antibody that binds the gp41-gp120 interface. *Nature* **515**, 138-142, doi:10.1038/nature13601 (2014).

4 Huang, J. *et al.* Broad and potent neutralization of HIV-1 by a gp41-specific human antibody. *Nature* **491**, 406-412, doi:10.1038/nature11544 (2012).

5 Wang, Y. *et al.* Combating the SARS-CoV-2 Omicron (BA.1) and BA.2 with potent bispecific antibodies engineered from non-Omicron neutralizing antibodies. *Cell discovery* **8**, 104, doi:10.1038/s41421-022-00463-6 (2022).

6 Wang, Y. *et al.* Novel sarbecovirus bispecific neutralizing antibodies with exceptional breadth and potency against currently circulating SARS-CoV-2 variants and sarbecoviruses. *Cell discovery* **8**, 36, doi:10.1038/s41421-022-00401-6 (2022).

7 Wu, F. *et al.* Antibody-dependent enhancement (ADE) of SARS-CoV-2 infection in recovered COVID-19 patients: studies based on cellular and structural biology analysis. *medRxiv*, 2020.2010.2008.20209114, doi:10.1101/2020.10.08.20209114 (2020).

8 Wang, Y. *et al.* Biparatopic antibody BA7208/7125 effectively neutralizes SARS-CoV-2 variants including Omicron BA.1-BA.5. *Cell discovery* **9**, 3, doi:10.1038/s41421-022-00509-9 (2023).

9 Zivanov, J. *et al.* New tools for automated high-resolution cryo-EM structure determination in RELION-3. *eLife* **7**, doi:10.7554/eLife.42166 (2018).

10 Zhang, K. Gctf: Real-time CTF determination and correction. *Journal of structural biology* **193**, 1-12, doi:10.1016/j.jsb.2015.11.003 (2016).

11 Punjani, A., Rubinstein, J. L., Fleet, D. J. & Brubaker, M. A. cryoSPARC: algorithms for rapid unsupervised cryo-EM structure determination. *Nature methods* **14**, 290-296, doi:10.1038/nmeth.4169 (2017).

12 Asarnow, D., Palovcak, E., Cheng, Y. UCSF pyem v0.5. Zenodo https://doi.org/10.5281/zenodo.3576630 (2019). doi:https://doi.org/10.5281/zenodo.3576630

13 Sanchez-Garcia, R. *et al.* DeepEMhancer: a deep learning solution for cryo-EM volume post-processing. *Communications biology* **4**, 874, doi:10.1038/s42003-021-02399-1 (2021).

14 Tan, Y. Z. *et al.* Addressing preferred specimen orientation in single-particle cryo-EM through tilting. *Nature Methods* **14**, 793-796, doi:10.1038/nmeth.4347 (2017).

15 Pettersen, E. F. *et al.* UCSF Chimera--a visualization system for exploratory research and analysis. *J Comput Chem* **25**, 1605-1612, doi:10.1002/jcc.20084 (2004).

16 Emsley, P., Lohkamp, B., Scott, W. G. & Cowtan, K. Features and development of Coot. *Acta Crystallogr D Biol Crystallogr* **66**, 486-501, doi:10.1107/s0907444910007493 (2010).

17 Afonine, P. V. *et al.* Real-space refinement in PHENIX for cryo-EM and crystallography. *Acta Crystallogr D Struct Biol* **74**, 531-544, doi:10.1107/s2059798318006551 (2018).

Table S1. Neutralization of 6i18 and S309 against a panel of 47 SARS-CoV-2 circulating single mutants.

SARS2 mutants	Fold change*	
	6i18	S309
WT	1.0	1.0
T307E	0.1	29.2
E309D	>977	>2252
V341I	6.4	4.3
F342L	>977	>2252
V367F	1.6	4.4
S371F	5.2	>2252
A372T	388.2	>2252
S373P	0.2	0.2
F374A	0.4	15.4
S375A	0.3	5.5
T376A	0.2	3.2
S383A	1.4	3.1
T385A	0.0	4.1
R408I	2.3	3.5
K417N	2.6	1.1
D427A	9.0	2.5
D428A	0.1	2.4
A435S	1.5	4.7
N439K	0.3	3.0
G446V	20.7	1.9
N450G	0.5	2.6
L452R	1.0	5.1
K458N	0.1	1.8
I472V	7.6	1.1
A475V	0.2	4.0
G476S	0.5	3.7
S477A	4.4	4.4
T478K	0.8	4.0
V483A	3.8	3.7
E484A	0.2	0.9
E484Q	0.6	3.2
G485A	0.5	0.5
G485R	0.4	2.8
F486A	0.2	0.9
F486L	1.7	2.7
F490L	0.6	3.4
P491A	>977	>2252
S494P	0.6	3.5
N501Y	0.2	1.6
Y508H	3.3	1.8
A570D	0.1	3.1
A570S	0.2	6.0
T572F	0.1	1.7
A575S	0.7	3.1
D614G	14.7	2.1
P681H	0.8	0.8
P681R	4.2	13.7
T716I	0.2	7.0
A831V	3.9	2.3
D950N	0.5	5.9
S982A	4.8	0.4

*Fold change is calculated as the IC50 of the mutant/the IC50 of WT. Mutants that decreased the sensitivity of 6i18 with fold change values between 10-100 are highlighted in yellow, and fold change values >100 are highlighted in red.

281 **Table S2. Cryo-EM data collection and refinement statistics.**
282

	XBB-S-6i18 complex
Data collection and processing	
Magnification	81000
Voltage (kV)	300
Total dose (e–/Å^2)	58
Defocus range (μm)	-1.2 to -2.5
Pixel size (Å)	0.82
Symmetry imposed	C1
Final particles (no.)	597,461
Map resolution (Å)	3.3
Refinement	
R.m.s. deviations	
Bond lengths (Å)	0.001
Bond angles (°)	0.398
Validation	
MolProbity score	2.45
Clashscore	10.22
Rotamer outlier (%)	3.78
Ramachandran plot	
Favored (%)	92.04
Allowed (%)	7.96
Disallowed (%)	0.00
EMDB	**36322**
PDB	**8JIO**

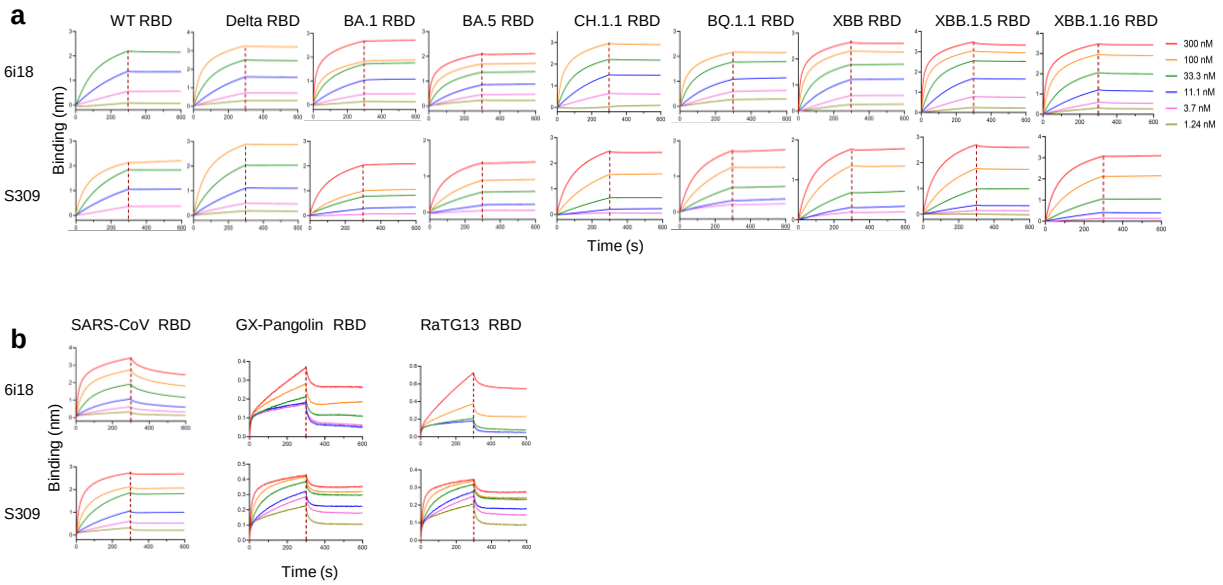

283

284 **Supplementary Fig. S1. Binding affinity of 6i18.** Binding affinities of 6i18 and
285 S309 to the RBDs of (**a**) SARS-CoV-2 variants as well as (**b**) other
286 sarbecoviruses as determined by BLI.

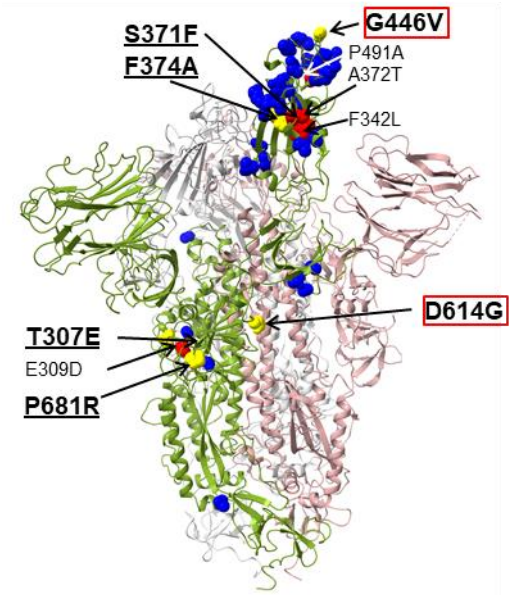

Supplementary Fig. S2. Three-dimensional representation of 47 SARS-CoV-2 circulating single mutants. Residues with 10-100 fold neutralization changes are highlighted in yellow, while residues with fold changes exceeding 100 are colored red. Unaffected residues are displayed in blue. Squares highlight mutants that specifically decreased 6i18 neutralization. Mutants conferring decreased sensitivity or resistance to S309 neutralization are underlined.

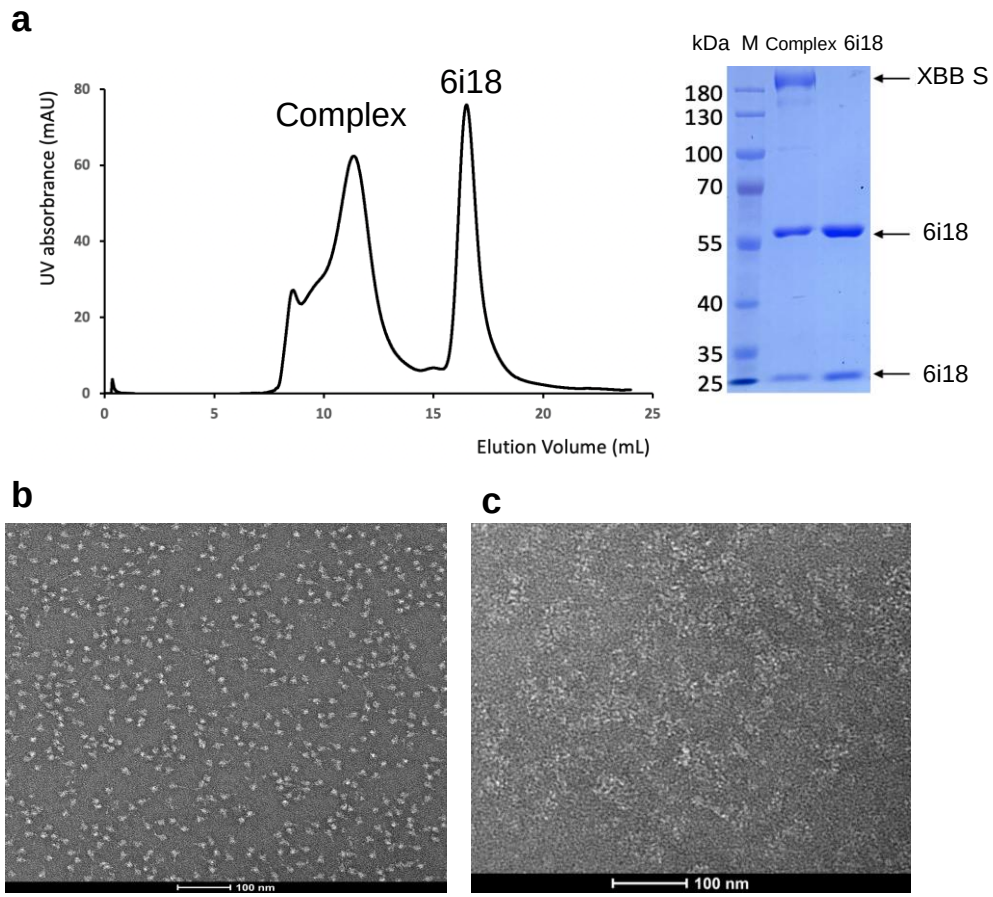

Supplementary Fig. S3. Negative staining EM image of SARS-CoV-2 XBB S in complex with 6i18. (**a**) Gel-filtration purification and SDS-PAGE of SARS-CoV-2 XBB S complexed with 6i18 complex. Negative staining EM images of (**b**) SARS-CoV-2 XBB S trimer alone and (**c**) S-6i18 complex, showing that binding of 6i18 disassembles SARS-CoV-2 XBB S trimer.

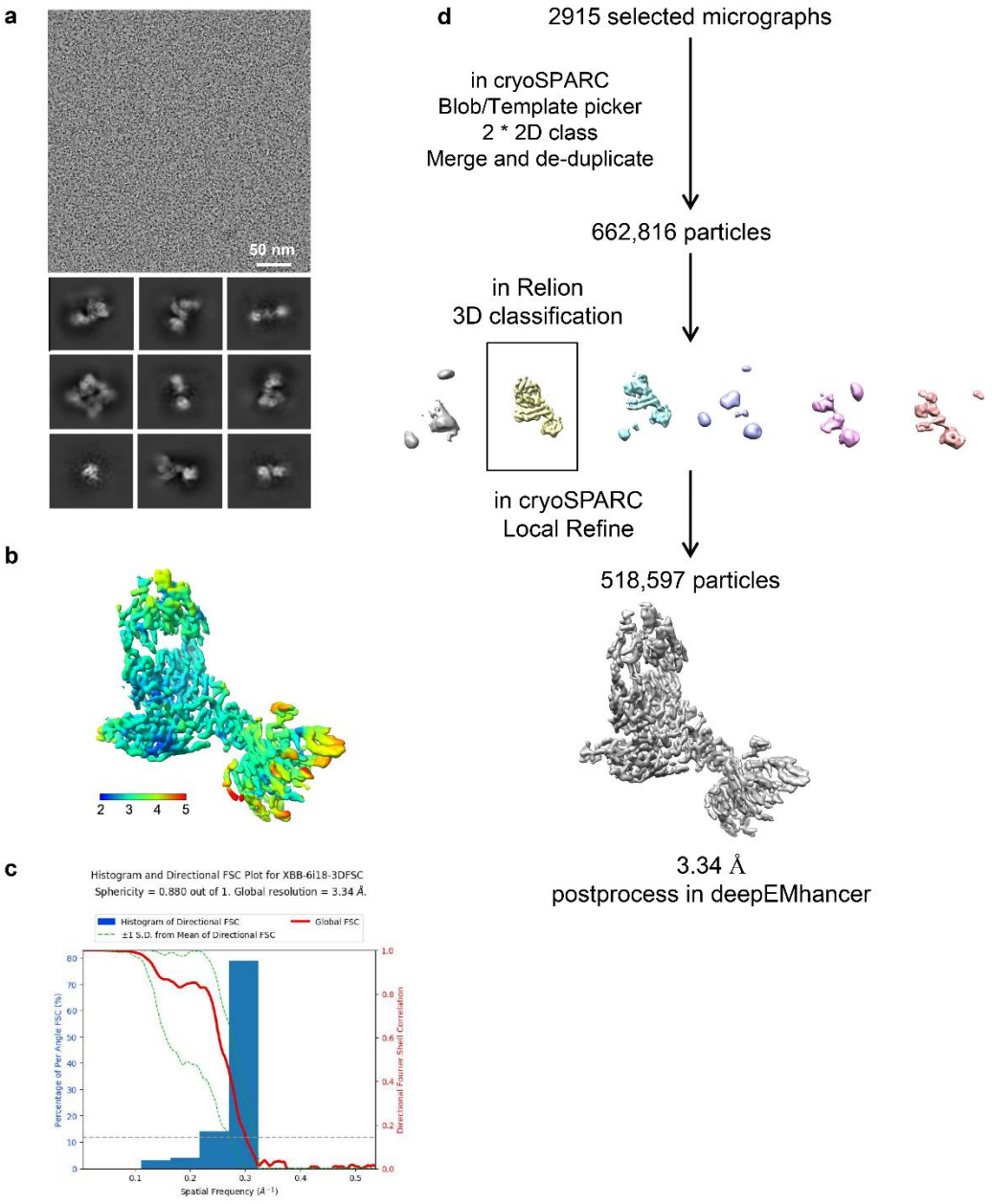

Supplementary Fig. S4. Cryo-EM data collection and processing of SARS-CoV-2 XBB S in complex with 6i18. (**a**) Representative electron micrograph and 2D classification results of 6i18 bound SARS-CoV-2 S. (**b**) Local resolution map for the reconstruction of NTD-RBD-6i18. (**c**) Histogram and FSC plot were generated using 3DFSC for the complex. The 0.143 cutoff is indicated by a horizontal dashed line. (**d**) Data processing flowchart of 6i18-bound SARS-CoV-2 XBB S.

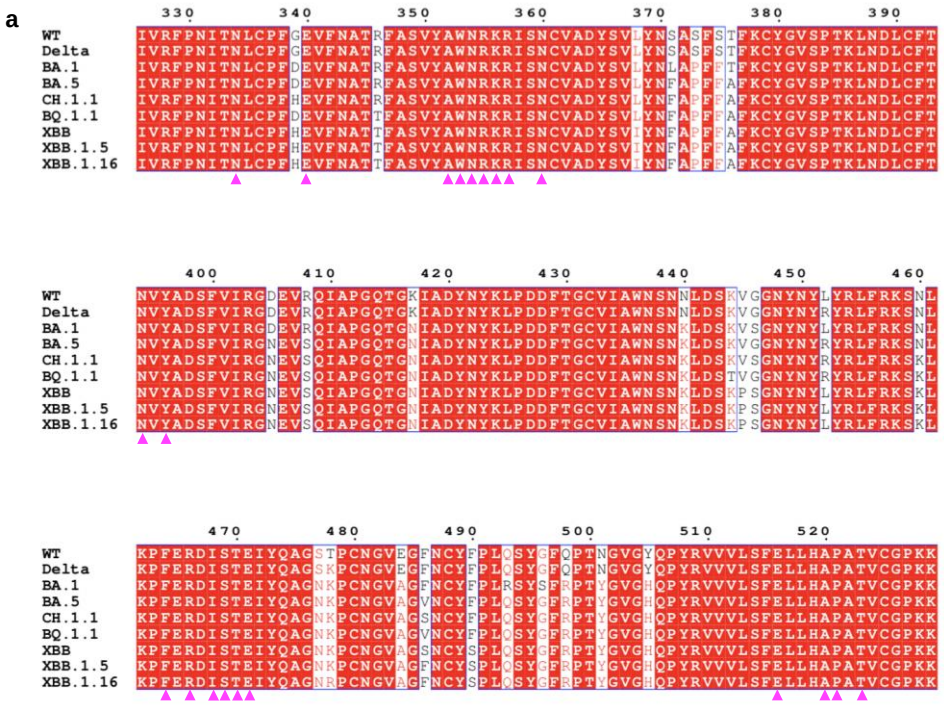

Supplementary Fig. S5. 6i18 epitope on S RBD. (a) Sequence alignment of WT, Delta, BA.1, BA.5, CH.1.1, BQ.1.1, XBB, XBB.1.5 and XBB.1.16 RBD. Conserved amino acids are highlighted as red. Residues involved in 6i18 binding are marked with magenta triangles. **(b)** Conservation rates of the residues involved in 6i18 binding across SARS-CoV-2 variants ranging from Jan 2020 through present circulating strains. (**c**) Structural comparison of 6i18

complexed with XBB S RBD and H-RBD class antibodies N-612-056 (PDBID: 7S0B), FD20 (PDBID: 7CYV), COVOX-45 (PDBID: 7PRY), WRAIR-2057 (PDBID: 7N4I), S2H97 (PDBID: 7M7W), ION-300 (PDBID: 7BNV) modelled onto XBB S RBD. (**d**) A comparison of neutralization activities of 6i18 and antibodies from the H-RBD class against the XBB.1.16 variant.